Nonlinear buckling of fibre-reinforced unit cells of lattice materials

Carlo Zschernack[a,*], M. Ahmer Wadee[b], Christina Völlmecke[a]

[a]*Stability and Failure of Functionally Optimized Structures Group, Institute of Mechanics, School V, Technische Universität Berlin, Sekr. MS 2, Einsteinufer 5, 10587 Berlin, Germany*
[b]*Department of Civil and Environmental Engineering, Imperial College London, South Kensington Campus, London SW7 2AZ, UK*

Abstract

Truss-based lattice materials are cellular materials with an outstanding potential for multi-functional use. This is owing to properties of high compressive strength to density ratios combined with a periodic and open structure. However, such structures at low relative densities are particularly vulnerable to elastic buckling failure. Fibre-reinforcement that increases the buckling strength of lattice materials is proposed and the behaviour of unit cells that are tessellated within the lattice is investigated. A two-dimensional square orientated unit cell and a three-dimensional tetrahedron-shaped unit cell are both modelled discretely using energy principles with the nonlinear interactive buckling behaviour being analysed. The analytical approach, based on a perturbation method, exhibits excellent agreement for the mechanical response when compared to results from numerical continuation for moderately large displacements. A fundamental understanding of the mechanical behaviour of a unit cell can be upscaled in future work. It is postulated that this will enable the determination of the constitutive behaviour of such lattice materials.

Keywords: mode interaction; analytical modelling; lattice materials; structural stability; nonlinear mechanics

1. Introduction

In the course of the last few decades, cellular materials, for example metallic foams or honeycombs, have emerged in various engineering applications, such as core materials in sandwich panels, due to the combination of advantageous mechanical, thermal and acoustic properties [1]. Recent progress in additive manufacturing has enabled the production of truss-based lattice materials that, according to [2], outperform other cellular materials particularly in terms of the strength-to-density ratio. Lattice materials tend to have periodic, open topologies that offer possibilities of combining structural functions with thermal application, as shown in [3], or in medical applications [4]. However, the compressive strength of such materials may be limited by the collapse mechanism of the respective unit cell from

---

*Corresponding author. Tel.: +49-(0)30-314-24214
Email address: `carlo.zschernack@tu-berlin.de` (Carlo Zschernack)

which the lattice material is composed. Cellular materials comprising slender trusses, and hence low relative densities, are known to be prone to elastic buckling of their internal structure [5]. In the current context, relative density $\bar{\rho}$ is defined by the expression:

$$\bar{\rho} = \frac{\rho^*}{\rho_{\mathrm{s}}}, \tag{1}$$

and refers to the ratio of the densities of the actual cellular material ρ^* to that of a solid body made from the parent material ρ_{s}. The correlation between low relative densities and an increased vulnerability to elastic buckling was demonstrated experimentally for different geometries and materials in [6] for $\bar{\rho} = 0.03$ and [7] for $\bar{\rho} = 0.014$. A mechanism for increasing the strength in axial compression that is widely applied in civil engineering is to reinforce compression members by introducing pretensioned elements such as cable stays. This leads to a higher buckling resistance as the cables help to restrain the structure against the initial displacement during buckling [8, 9, 10, 11, 12, 13]. By transferring this concept towards lattice materials the maximum compressive strength can be potentially increased beyond the conventional eigenvalue buckling load while avoiding a considerable gain in self-weight, or in the current case avoiding a significant increase in $\bar{\rho}$.

The objective of the current work is to investigate the potential effect of interwoven fibres on the critical and post-buckling response of lattice materials. Therefore, a fibre-reinforced lattice material is proposed based on an existing square orientated lattice material discussed in [6]. The deformational behaviour of the unit cell in the internal structure under axial compression is investigated using an analytical approach focusing on elastic buckling behaviour in the nonlinear range. Discrete models of unit cells comprising rigid links and springs, initially in two-dimensions and subsequently in three-dimensions are formulated using total potential energy principles. The performance of each model is evaluated in terms of the critical and post-buckling behaviour both analytically and numerically. Potentially important nonlinear interactions between different instability modes in the post-buckling range and the consequences to the overall stability are investigated. It has been demonstrated previously that a fundamental understanding of system behaviour can facilitate exploitation of these lightweight materials with safety [14]. The article concludes with a discussion where some detailed suggestions for further work are made.

2. Fibre-reinforced square orientated lattice material

2.1. Material development

Figure 1 shows a square orientated lattice material suggested and experimentally evaluated with respect to its out-of-plane compressive behaviour in [6]. Figure 1(b) emphasises the vulnerability to elastic buckling failure of the internal structure with low relative densities. This failure mechanism may be suppressed by a square lattice structure which is reinforced by fibres. The fibres contribute to the buckling resistance and hence to the overall compressive strength of the lattice material. A computer aided design (CAD) model of such a fibre-reinforced lattice material is presented in Fig. 2.
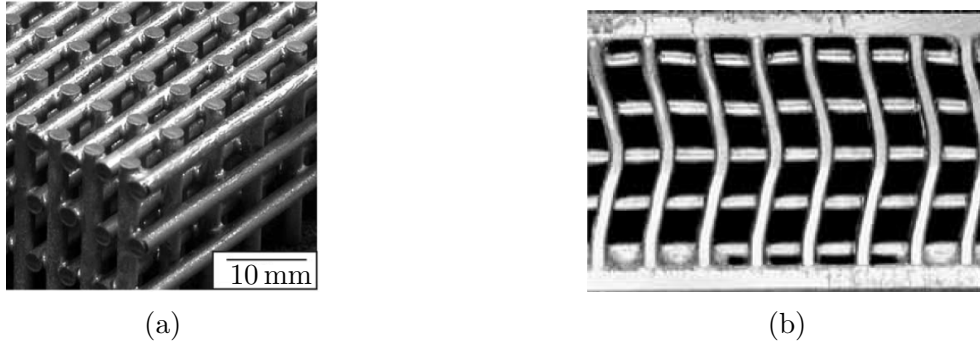
Figure 1: Photographs of a square orientated lattice material showing (a) the geometry and (b) the deformational behaviour exhibiting fibre buckling within the internal structure [6].
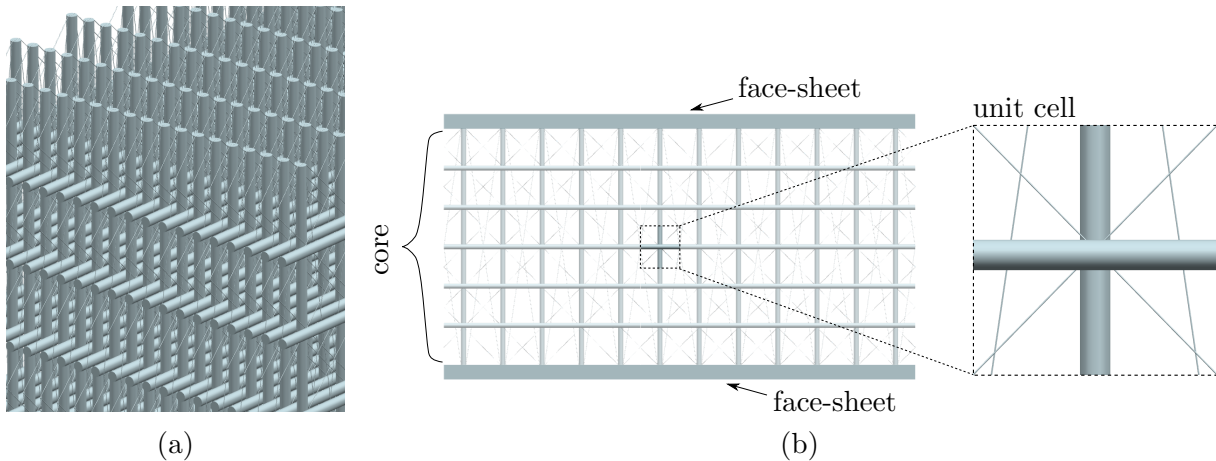

Figure 2: CAD model of a fibre-reinforced lattice material showing its (a) structure and (b) application as a sandwich core.

2.2. Model development

A unit cell of the internal fibre-reinforced structure is modelled to obtain a deeper understanding of the deformational behaviour at cell level during elastic buckling. Therefore, a cross-shaped unit cell, as highlighted in Fig. 2(b), is modelled as a multiple-degree-of-freedom system in two dimensions, as represented in Fig. 3. The horizontal and vertical struts are modelled by pin-jointed rigid links, whereas the joints are reinforced by rotational springs of stiffness c_y. The horizontal strut is connected to the vertical strut at mid-height rigidly. Moreover, a lateral spring acts with stiffness k at mid-height of the horizontal strut to model the lateral resistance contributed by the interwoven fibres. The cell is assumed to be fully fixed at the upper and lower ends. Hence, the x-displacement and rotation of the outer links of length a is prevented such that they remain vertical. The respective ends of the horizontal crossarm, assigned with length b, are allowed to move in the x- as well as the z-direction. However, it is assumed that they remain horizontal as well as at the same height as the rigid corner. This enables the comprehensive description of the deformational behaviour at the cell level using only two generalized coordinates q_1, q_2.
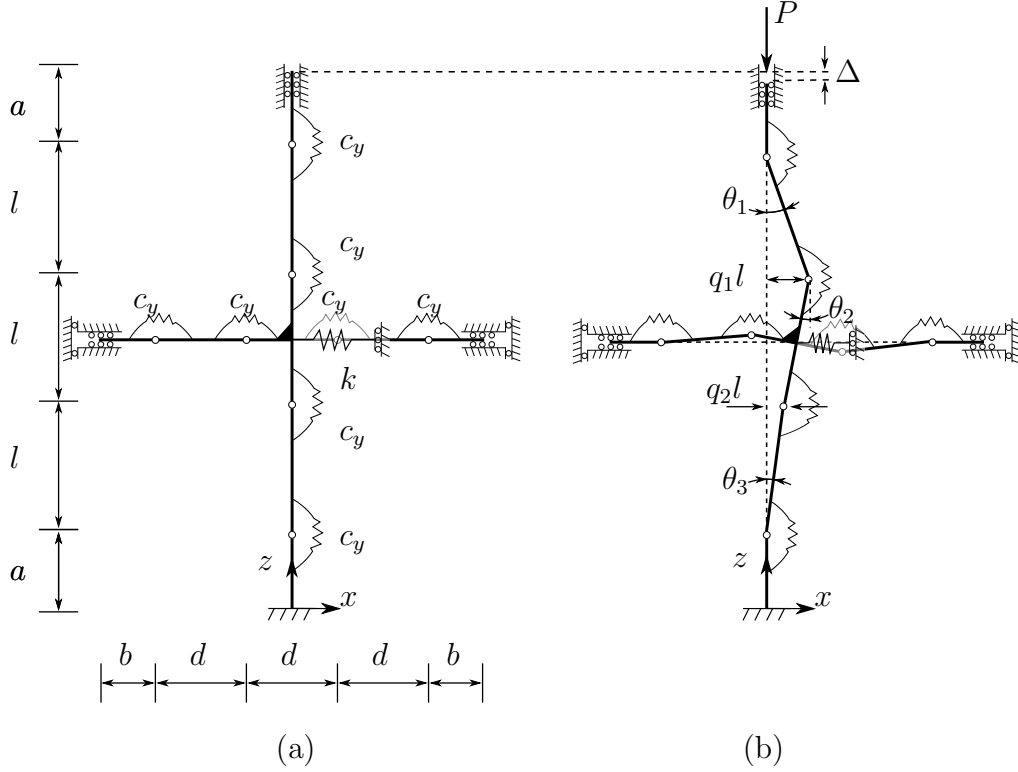
3

Figure 3: (a) Configuration of the undeflected rigid link model for the unit cell shown in Fig. 2(b), and (b) an arbitrarily deflected state under axial load P.

In the case where one cell would be embedded into a grid of many cells, the constraints arising from the neighbouring cells would need to be considered also.

2.3. Total Potential Energy

The total potential energy function V for a single cell is formulated by evaluating the total strain energy stored in all the springs U and the work done by the external load $P\Delta$ [15]:

$$V(q_i, P) = U(q_i) - P\Delta(q_i) \tag{2}$$

where currently $i = \{1, 2\}$. The total strain energy is decomposed into two constituent parts, the contribution from the longitudinal springs U_L and those from the rotational springs U_R. These terms are developed by considering an arbitrarily deflected state in the xz-plane, as shown in Fig. 3(b). The energy stored in the lateral spring gives the expression:

$$U_L = \frac{kl^2}{8} (q_1 + q_2)^2 . \tag{3}$$

For the strain energy stored in the rotational springs, the behaviour of the horizontal strut becomes significant due to the rigid joint at mid-height. Hence, U_R consists of one

4

component being active, *i.e.* non-zero, for every deflected shape and a second component being non-zero only for buckling shapes where $q_1 \neq q_2$. This leads to the expression:

$$U_\text{R} = \frac{c_y}{2} \left[\theta_1^2 + \theta_3^2 + \theta_4^2 + \theta_6^2 + (\theta_1 - \theta_2)^2 + (\theta_2 + \theta_3)^2 + (\theta_4 - \theta_5)^2 + (\theta_5 + \theta_6)^2 \right], \quad (4)$$

in which:

$$\theta_1 = \arcsin(q_1), \quad \theta_2 = \arcsin(q_2 - q_1), \quad \theta_3 = \arcsin(q_2),$$

$$\theta_4 = \arcsin\left(\frac{q_1 - q_2}{2}\right), \quad \theta_5 = \arcsin(q_2 - q_1), \quad \theta_6 = \arcsin\left(\frac{q_2 - q_1}{2}\right).$$

The end-shortening displacement Δ contributes to the work done by the load P and is given by the expression:

$$\Delta = l \left[3 - \left(\sqrt{1 - q_1^2} + \sqrt{1 - (q_2 - q_1)^2} + \sqrt{1 - q_2^2} \right) \right]. \quad (5)$$

Assuming only moderately large deformations, the energy is expressed as a power series and is truncated after order four. The total potential energy V can be non-dimensionalized by dividing through the rotational stiffness c_y, thus:

$$\tilde{V}(q_1, q_2, p) = \frac{11}{2} q_1^2 - 9 q_1 q_2 + \frac{13}{2} q_1^2 q_2^2 - \frac{9}{2} q_1^3 q_2 + \frac{11}{2} q_2^2 - \frac{9}{2} q_1 q_2^3 + \frac{19}{12} \left(q_1^4 + q_2^4 \right) + \frac{K}{8} \left(q_1^2 + q_2^2 \right.$$
$$\left. + 2 q_1 q_2 \right) - p \left(q_1^2 - q_1 q_2 + \frac{3}{4} q_1^2 q_2^2 - \frac{1}{2} q_1^3 q_2 + q_2^2 - \frac{1}{2} q_1 q_2^3 + \frac{1}{4} q_1^4 + \frac{1}{4} q_2^4 \right), \quad (6)$$

with the now non-dimensionalized parameters given by:

$$\tilde{V} = \frac{V}{c_y}, \quad K = \frac{k l^2}{c_y}, \quad p = \frac{P l}{c_y}.$$

The potential energy expression is also diagonalized using the following transformation:

$$u_1 = q_1 + q_2, \quad u_2 = q_1 - q_2. \quad (7)$$

This results in the diagonalized non-dimensional total potential energy expression $A(u_1, u_2, p)$:

$$A(u_1, u_2, p) = \frac{1}{2} u_1^2 + 5 u_2^2 + \frac{3}{8} u_1^2 u_2^2 + \frac{1}{24} u_1^4 + \frac{7}{6} u_2^4 + \frac{K}{8} u_1^2$$
$$- \frac{p}{4} \left(u_1^2 + 3 u_2^2 + \frac{3}{8} u_1^2 u_2^2 + \frac{1}{16} u_1^4 + \frac{9}{16} u_2^4 \right). \quad (8)$$

2.4. Critical equilibrium

The normalized critical loads p_i^C of two different buckling modes are subsequently calculated through linear eigenvalue analysis where the Hessian matrix of A becomes singular, thus:

$$\det(\mathbf{A}) = A_{11}^\text{F} A_{22}^\text{F} = 0 \quad (9)$$

5

with $A_{ij}^{\mathrm{F}} = \left(\frac{\partial^2 A}{\partial u_i \partial u_j} \right)$ being evaluated along the fundamental equilibrium path F, which in this case can be determined to be $q_1 = q_2 = 0$ and hence $u_1 = u_2 = 0$. The associated buckling modes are determined through the calculation of the respective eigenvectors $\vec{a}_i$:

$$
\begin{aligned}
p_1^{\mathrm{C}} &= \frac{1}{2}K + 2, \quad \vec{a}_1 = [1, 0]^{\mathrm{T}} \quad \Rightarrow \quad q_1 = q_2 \\
p_2^{\mathrm{C}} &= \frac{20}{3}, \quad \vec{a}_2 = [0, 1]^{\mathrm{T}} \quad \Rightarrow \quad q_1 = -q_2.
\end{aligned}
\tag{10}
$$

In the following discussion, mode 1 will be referred to as the symmetric mode with the active coordinate u_1, whereas mode 2 will be referred to as the antisymmetric mode with u_2 being the active coordinate. The critical loads are plotted in Fig. 4 against the normalized
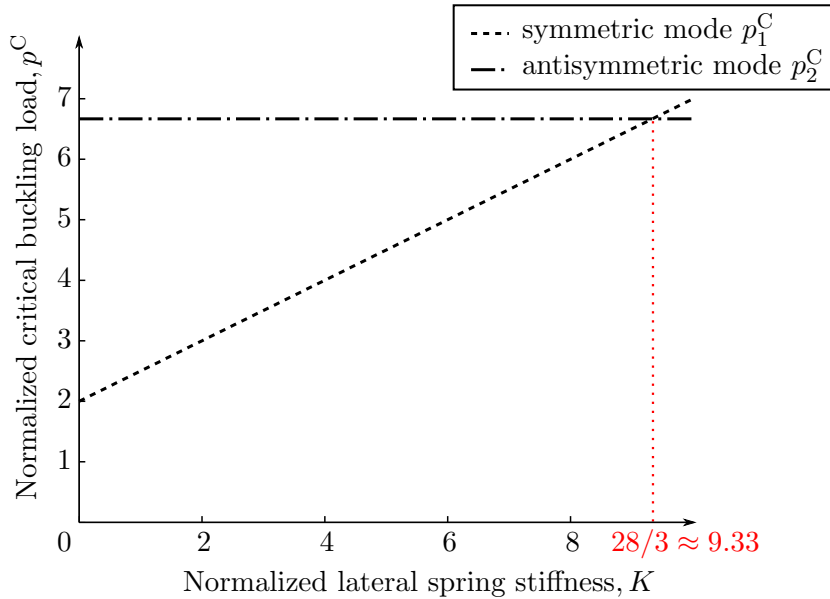

Figure 4: Distribution of critical loads p_i^{C} in terms of K.

lateral stiffness parameter K. Note that p_2^{C} is independent of K because the midspan lateral displacement is zero in the antisymmetric mode. Moreover, note that $p_1^{\mathrm{C}} = p_2^{\mathrm{C}}$ when $K = 28/3$ and mode 2 is critical when $K > 28/3$.

2.5. Post-buckling behaviour

According to the perturbation method introduced in [16] and [17], the equilibrium equations derived from the truncated potential energy expression in Eq. (8) can be written

6

in general form:

$$
\begin{aligned}
\frac{\partial A}{\partial u_1} &= A^{\mathrm{F}}_{11}u_1 + \frac{1}{2}A^{\mathrm{F}}_{1122}u_1u_2^2 + \frac{1}{6}A^{\mathrm{F}}_{1111}u_1^3 + \delta p A'^{\mathrm{F}}_{11}u_1 = 0, \\
\frac{\partial A}{\partial u_2} &= A^{\mathrm{F}}_{22}u_2 + \frac{1}{2}A^{\mathrm{F}}_{1122}u_1^2u_2 + \frac{1}{6}A^{\mathrm{F}}_{2222}u_2^3 + \delta p A'^{\mathrm{F}}_{22}u_2 = 0,
\end{aligned}
\tag{11}
$$

where $\delta p = p - p_0$ is a load increment in p from an arbitrary load level p_0. The respective coefficients are:

$$
\begin{aligned}
A^{\mathrm{F}}_{11} &= \frac{1}{4}K + 1 - \frac{1}{2}p_0, \quad A^{\mathrm{F}}_{22} = 10 - \frac{3}{2}p_0, \quad A^{\mathrm{F}}_{1122} = \frac{3}{2} - \frac{3}{8}p_0, \\
A^{\mathrm{F}}_{1111} &= 1 - \frac{3}{8}p_0, \quad A^{\mathrm{F}}_{2222} = 28 - \frac{27}{8}p_0 \quad A'^{\mathrm{F}}_{11} = -\frac{1}{2}, \quad A'^{\mathrm{F}}_{22} = -\frac{3}{16}.
\end{aligned}
\tag{12}
$$

To find a relationship between u_1 and u_2, both equilibrium equations from Eq. (11) are respectively solved for δp and subsequently equated. The resulting relationship:

$$
u_1^2\left(\frac{1}{6}\frac{A^{\mathrm{F}}_{1111}}{A'^{\mathrm{F}}_{11}} - \frac{1}{2}\frac{A^{\mathrm{F}}_{1122}}{A'^{\mathrm{F}}_{22}}\right) + u_2^2\left(\frac{1}{2}\frac{A^{\mathrm{F}}_{1122}}{A'^{\mathrm{F}}_{11}} - \frac{1}{6}\frac{A^{\mathrm{F}}_{2222}}{A'^{\mathrm{F}}_{22}}\right) = \frac{A^{\mathrm{F}}_{22}}{A'^{\mathrm{F}}_{22}} - \frac{A^{\mathrm{F}}_{11}}{A'^{\mathrm{F}}_{11}},
\tag{13}
$$

reveals that the post-buckling behaviour will be either elliptic or hyperbolic-shaped as it follows the specific form

$$
a_1 u_1^2 + a_2 u_2^2 = a_3
\tag{14}
$$

which gives

- a hyperbola branching from the u_1-axis for $a_1, a_3 > 0, a_2 < 0$ or $a_1, a_3 < 0, a_2 > 0$,

- a hyberbola branching from the u_2-axis for $a_1 < 0, a_2, a_3 > 0$ or $a_1 > 0, a_2, a_3 < 0$,

- straight lines through the origin for $a_1 > 0, a_2 < 0, a_3 = 0$ or $a_1 < 0, a_2 > 0, a_3 = 0$ or

- an ellipse for $a_1, a_2, a_3 > 0$.

Hence, the characteristic of the post-buckling behaviour depends on the magnitude and signs of the respective terms a_1, a_2, a_3. If $p_0 = p_1^{\mathrm{C}}$ the solution in the u_1u_2-plane can be rewritten thus:

$$
u_1^2\underbrace{\left(\frac{1}{6}A^{\mathrm{F}}_{1111} - \frac{1}{2}A^{\mathrm{F}}_{1122}\frac{A'^{\mathrm{F}}_{11}}{A'^{\mathrm{F}}_{22}}\right)}_{a_1} + u_2^2\underbrace{\left(\frac{1}{2}A^{\mathrm{F}}_{1122} - \frac{1}{6}A^{\mathrm{F}}_{2222}\frac{A'^{\mathrm{F}}_{11}}{A'^{\mathrm{F}}_{22}}\right)}_{a_2} = \underbrace{-\Delta p A'^{\mathrm{F}}_{11}}_{a_3},
\tag{15}
$$

where $\Delta p = p_2^{\mathrm{C}} - p_1^{\mathrm{C}}$. Since only moderately large deflections are considered and Δp obviously influences the distance of the coupled-buckling curve from the origin, the following

considerations are limited to values of K within the vicinity of $K = 28/3$ where $\Delta p = 0$. Within this region it is valid since:

$$A_{1111}^{\mathrm{F}} > 3A_{1122}^{\mathrm{F}}\frac{A_{11}'^{\mathrm{F}}}{A_{22}'^{\mathrm{F}}} \Rightarrow a_1 > 0$$

$$A_{2222}^{\mathrm{F}} > 3A_{1122}^{\mathrm{F}}\frac{A_{22}'^{\mathrm{F}}}{A_{11}'^{\mathrm{F}}} \Rightarrow a_2 < 0. \tag{16}$$

Hence, the form of coupled buckling is determined solely by the term $a_3 = -\Delta p A_{11}'^{\mathrm{F}}$. Since $A_{11}'^{\mathrm{F}}$ is a constant, Table 1 shows the possible forms of interactive buckling for moderately
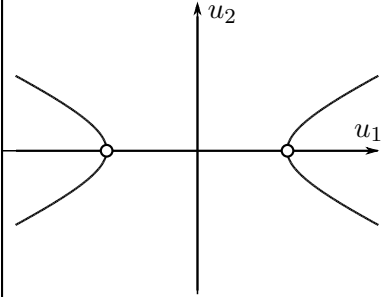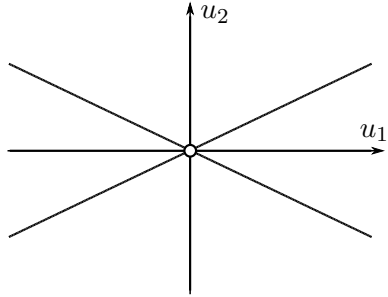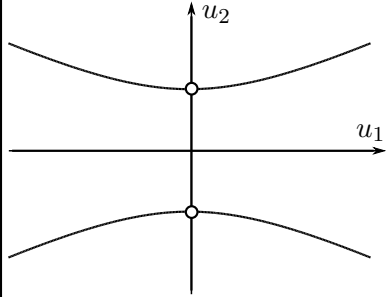
$K = 9.30\,(\Delta p < 0)$ symmetric mode critical	$K = 28/3\,(\Delta p = 0)$ compound branching point	$K = 9.40\,(\Delta p > 0)$ antisymmetric mode critical
hyperbola branching from u_1-axis	straight lines going through origin	hyperbola branching from u_2-axis

Table 1: Forms of the coupled solutions for the symmetric and antisymmetric modes being critical and simultaneous.

large deflections solely dependent on Δp. The equilibrium paths for the case where $K = 28/3$ are shown in Fig. 5. Note that the paths showing interactive buckling are less stable than those from the pure modes.

3. Tetrahedron-shaped unit cell

The previous section began on the material level and focused then on the derivation and modelling of a representative element taken from the proposed fibre-reinforced square orientated lattice material. The current section considers an element that comprises two tetrahedrons shaping a fibre-reinforced unit cell in three dimensions (Fig. 6). Owing to its regular geometry, it can be reproduced periodically to manufacture a lattice material. Considering the increasing advances in the technology of additive manufacturing, the current work could be considered as groundwork for the future development of this range of lattice materials. Therefore, the unit cell is devised, structurally analysed under axial compression and compared to the element in the previous section.
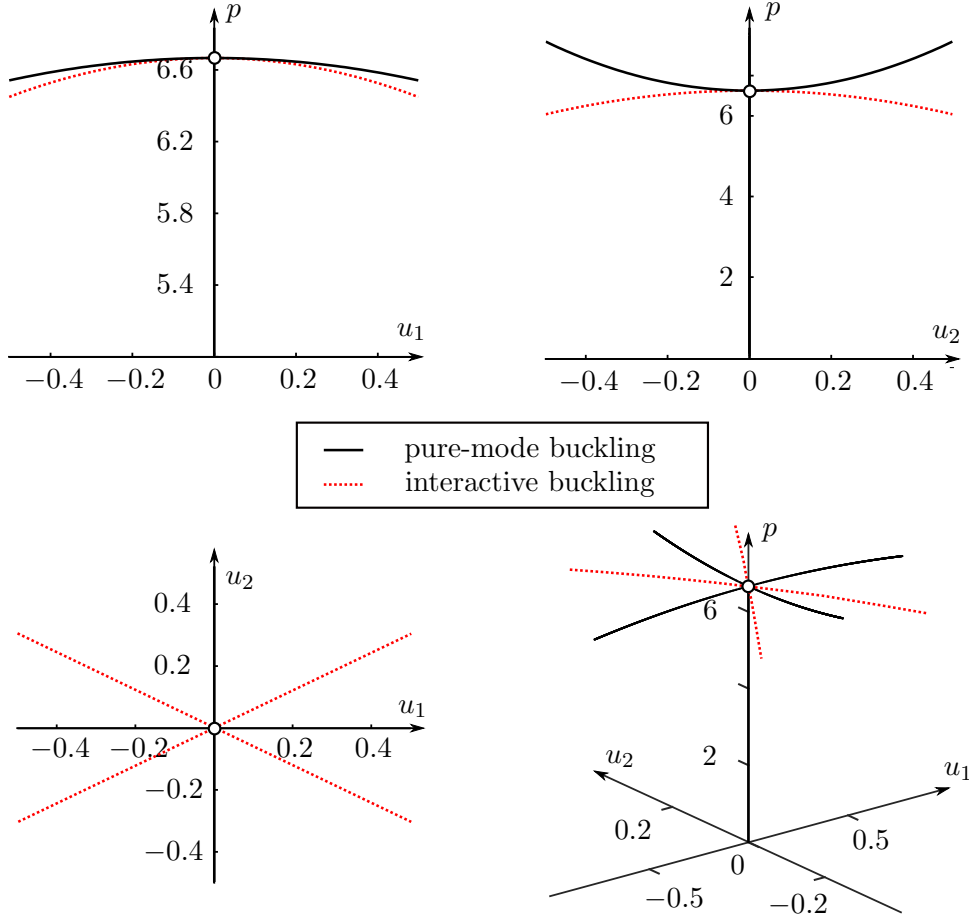
Figure 5: Pure and coupled buckling for $K = 28/3$. Note that the interactive buckling branches are less stable than those from the pure buckling modes.

3.1. Model development

The unit cell is modelled by discretizing it into a three-dimensional multiple degree-of-freedom system. The unit cell, as illustrated in Fig. 6, comprises a slender column equipped with three crossarms at mid-height. The ends of the crossarms are connected with the tips of the column by fibres. The discrete model of the unit cell is shown in Fig. 7; it comprises three nodes and four rigid links of length l. The rotational movement at the nodes is restrained by rotational springs of stiffness c_x and c_y which respectively represent the flexural rigidity about the x- and y-axis. A rosette of three lateral springs of stiffness k and natural length a is positioned at the central node to model the resistance against buckling from the fibre-supported crossarms. The displacements at every node are given by $q_{ix}l$ and $q_{iy}l$ for $i = \{1, 2, 3\}$ with q_{ix} and q_{iy} as non-dimensional generalized coordinates. Hence, the system has six degrees of freedom: three concerning deflection in the x-direction and a further three for the y-direction respectively.
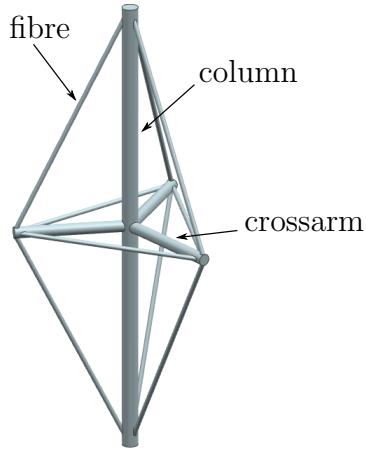
Figure 6: Unit cell comprising two tetrahedrons forming a fibre-supported lattice.
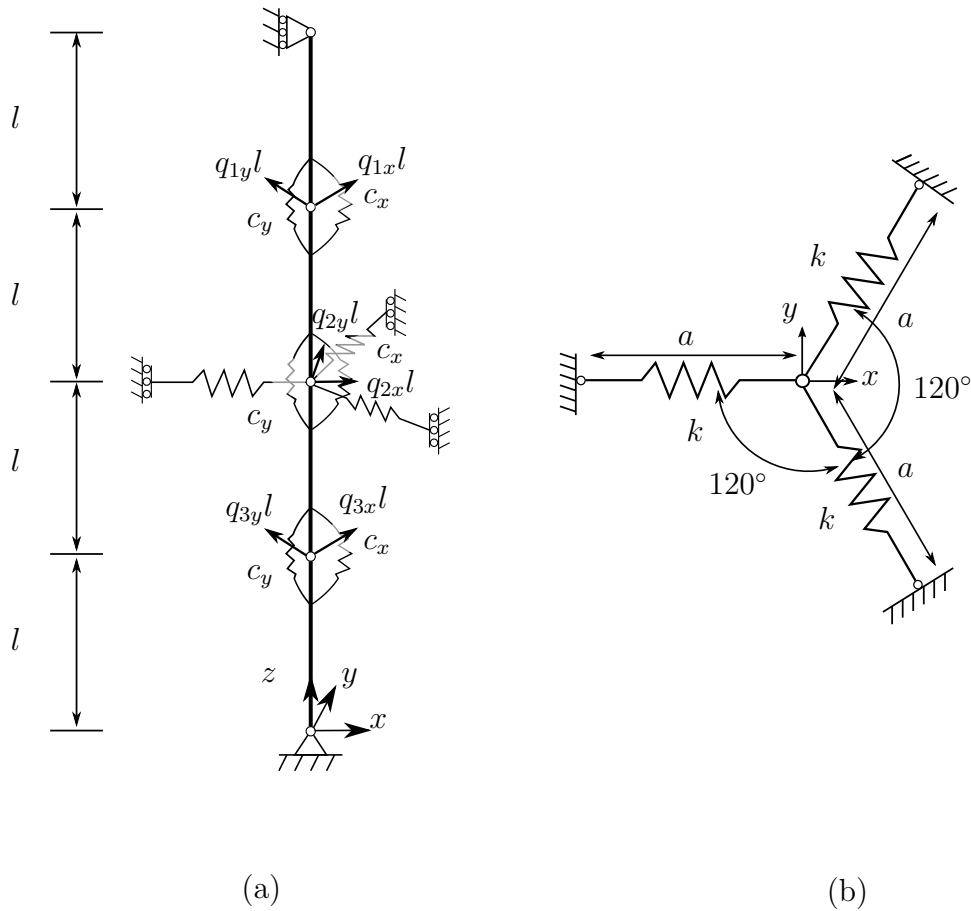

(a)

(b)

Figure 7: Model comprising rigid links and springs for the tetrahedron shaped unit cell in (a) an isometric view and (b) a plan view of mid-section spring rosette that resists lateral displacement.

3.2. Total potential energy

The equilibrium equations are again determined according to the minimum total potential energy principle. The strain energy from the longitudinal springs U_L is developed by considering an arbitrarily deflected state in the xy-plane, which has the general form:

$$U_L = \frac{k}{2} \sum_{i=1}^{3} (a - l_i)^2, \tag{17}$$

where a is the rosette link natural length and l_i is the current length in the deflected state. The expression for U_L is derived by means of Fig. 8 and is given by the expression:
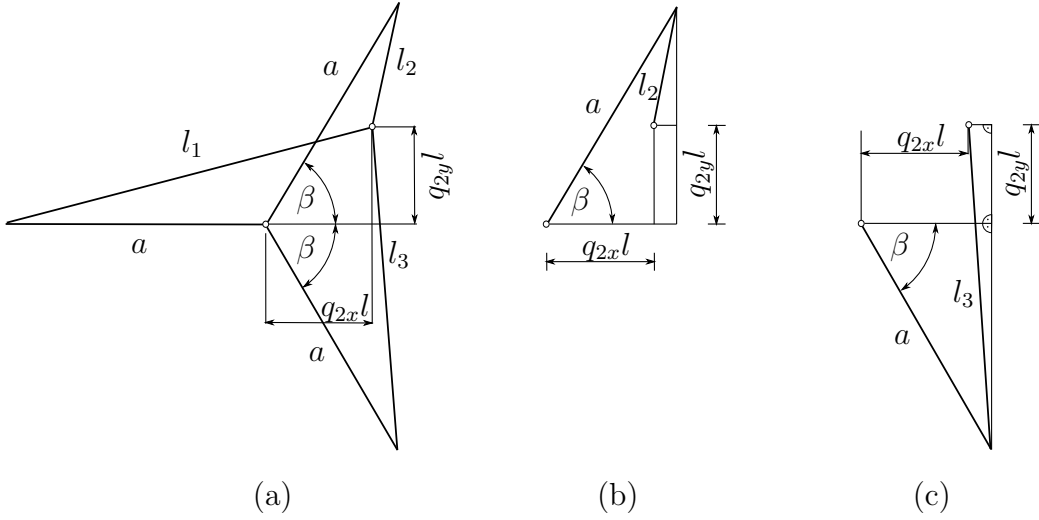

Figure 8: Calculation of strain energy stored in the spring rosette: (a) change in length of all elements; (b–c) deflection of individual rosette link elements.

$$U_L = \frac{kl^2}{2} \left[\left(\sqrt{(\alpha + q_{2x})^2 + q_{2y}^2} - \alpha \right)^2 + \left(\sqrt{\left(\sqrt{3}\,\alpha/2 - q_{2y} \right)^2 + (\alpha/2 - q_{2x})^2} - \alpha \right)^2 \right.$$
$$\left. + \left(\sqrt{\left(\sqrt{3}\,\alpha/2 + q_{2y} \right)^2 + (\alpha/2 - q_{2x})^2} - \alpha \right)^2 \right], \tag{18}$$

where $\alpha = a/l$.

The strain energy contribution of the rotational springs can be derived from Fig. 9(a), which is analogous to the formulation in [18], and is given by the expression:

$$U_R = \frac{c_y}{2} \left\{ \left[(\theta_{0x} - \theta_{1x})^2 + (\theta_{1x} + \theta_{3x})^2 + (\theta_{4x} - \theta_{3x})^2 \right] \right.$$
$$\left. + R \left[(\theta_{0y} - \theta_{1y})^2 + (\theta_{1y} + \theta_{3y})^2 + (\theta_{4y} - \theta_{3y})^2 \right] \right\}, \tag{19}$$
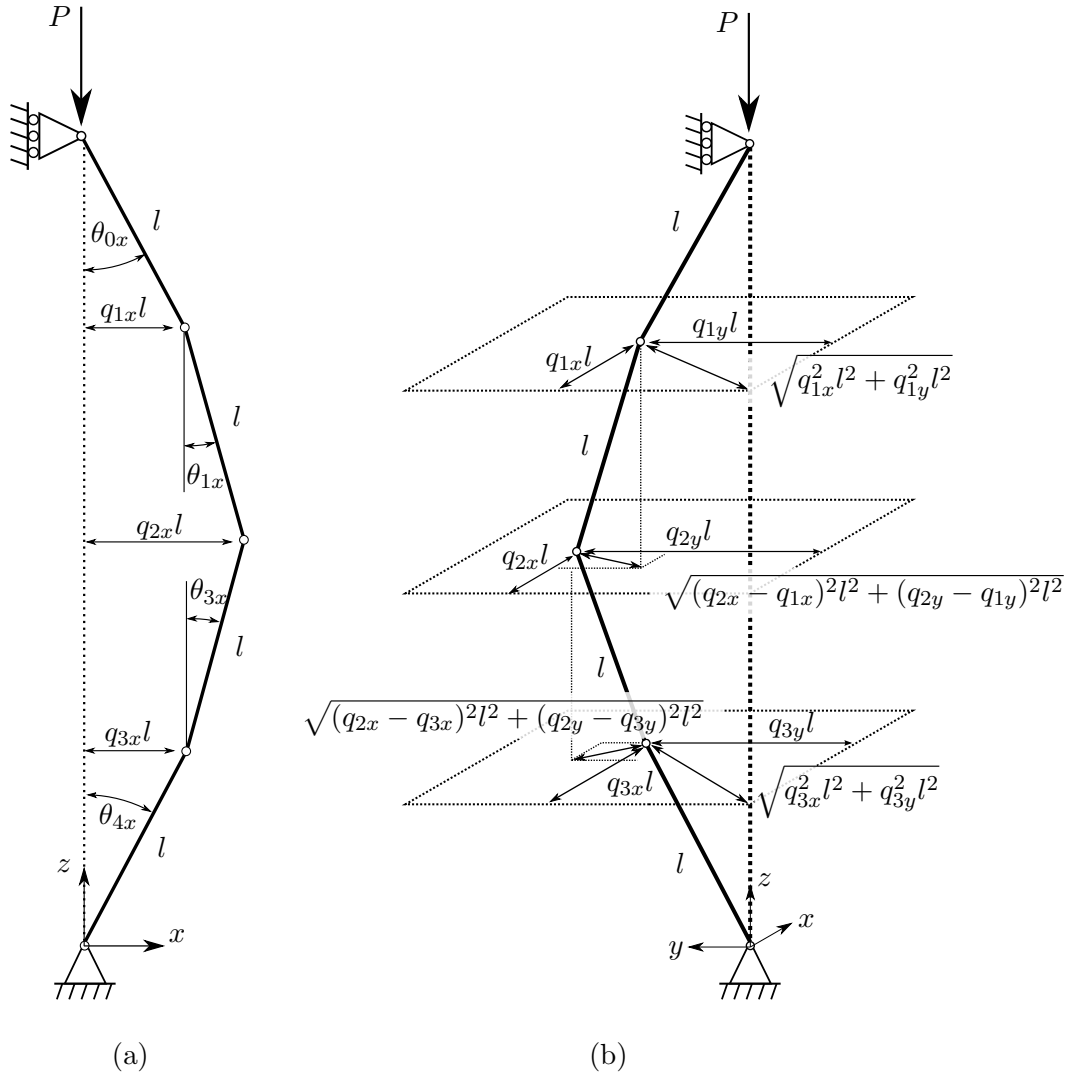
Figure 9: (a) Angles of rotation about the y-axis ; (b) evaluation of the vertical end-shortening to calculate the work done by the load P.

where:

$$R = c_x/c_y, \quad \theta_{0y} = \arcsin(q_{1y}), \quad \theta_{1y} = \arcsin(q_{2y} - q_{1y}),$$
$$\theta_{3y} = \arcsin(q_{2y} - q_{3y}), \quad \theta_{4y} = \arcsin(q_{3y}), \quad \theta_{0x} = \arcsin(q_{1x}), \tag{20}$$
$$\theta_{1x} = \arcsin(q_{2x} - q_{1x}), \quad \theta_{3x} = \arcsin(q_{2x} - q_{3x}), \quad \theta_{4x} = \arcsin(q_{3x}).$$

The total strain energy is given by the expression:

$$U = U_\mathrm{L} + U_\mathrm{R}. \tag{21}$$

The work done by the load term $P\Delta$ is also calculated using a procedure analogous to the three-dimensional link model by [18] and has the expression thus:

$$P\Delta = Pl\left\{ 4 - \left[\sqrt{1 - (q_{1x}^2 + q_{1y}^2)} + \sqrt{1 - (q_{2x} - q_{1x})^2 - (q_{2y} - q_{1y})^2} \right. \right.$$
$$\left. \left. + \sqrt{1 - (q_{2x} - q_{3x})^2 - (q_{2y} - q_{3y})^2} + \sqrt{1 - (q_{3x}^2 + q_{3y}^2)} \right] \right\}. \tag{22}$$

3.3. Critical equilibrium

Prior to determining the critical and post-buckling behaviour, the energy formulation is truncated beyond order 4 once more. Subsequently the expression is diagonalized by changing the set of variables from q_{ix}, q_{iy} for $i = \{1, 2, 3\}$ to the pure modal-coordinates u_j for $j = \{1, 2 \ldots, 6\}$ as presented in Appendix A. Hence, the diagonalized potential energy expression becomes a function A dependent on those new coordinates as well as on the load parameter p; hence

$$A = A(u_1, u_2, \ldots, u_6, p). \tag{23}$$

Linear eigenvalue analysis, as in the previous section, yields the following normalized critical loads:

$$p_1^\mathrm{C} = 2 + \frac{3}{4}K - \frac{1}{4}\sqrt{32 - 24K + 9K^2}$$
$$p_2^\mathrm{C} = 2$$
$$p_3^\mathrm{C} = 2 + \frac{3}{4}K + \frac{1}{4}\sqrt{32 - 24K + 9K^2}$$
$$p_4^\mathrm{C} = 2R + \frac{3}{4}K - \frac{1}{4}\sqrt{32R^2 - 24KR + 9K^2} \tag{24}$$
$$p_5^\mathrm{C} = 2R$$
$$p_6^\mathrm{C} = 2R + \frac{3}{4}K + \frac{1}{4}\sqrt{32R^2 - 24KR + 9K^2}.$$

The individual elements of the Hessian matrix $\mathbf{A}$ of the potential energy normalized by dividing through by c_y are listed in Appendix B. The loads triggering modes 1 and 4, modes 2 and 5, and modes 3 and 6 would respectively coincide for the case $R = 1$. It is observed, that modes 1 and 4 are critical for small K, whereas for larger K modes 2 and
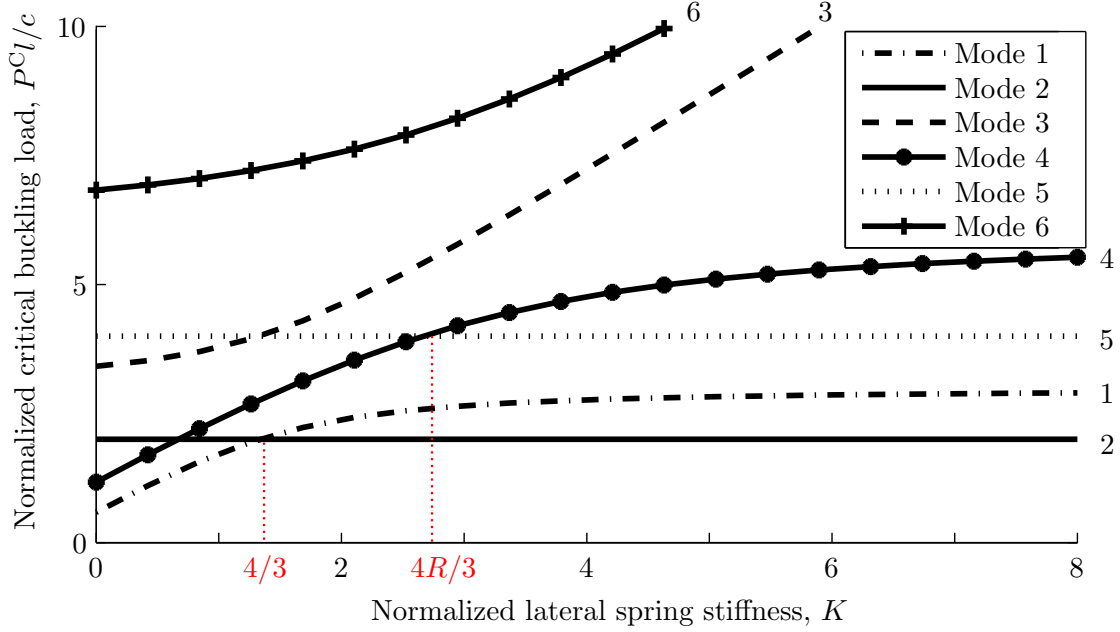
Figure 10: Distribution of critical loads in terms of K for an example where $R = 2$.

5 become critical. For the sake of clarity the critical loads have been plotted in Fig. 10 against the non-dimensional parameter of lateral stiffness K for the case where $R = 2$. The respective eigenvectors are also calculated (see Appendix C). The shapes of the six modes are illustrated in Fig. 11, where λ_i expressions for $i = \{1, 3, 4, 6\}$ are dependent on
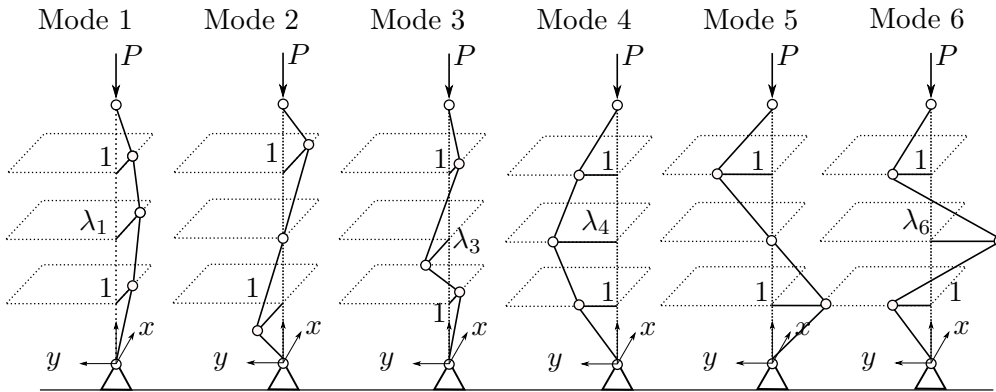

Figure 11: Discrete buckling eigenmodes for the tetrahedron unit cell link model.

R and K as found in Eq. (A.2).

3.4. Modal interactions

The results for mode interaction between both symmetric and antisymmetric modes are now presented. Under the assumption that the configuration of the model parameters

14

separates the bifurcation points of the remaining modes sufficiently, the remaining modes are considered to be non-active. Hence, the set of governing equilibrium equations is reduced; later, however, the full system of untruncated equations is solved numerically for validation purposes.

3.4.1. Symmetric modes

For the investigation of the interaction of modes 1 and 4 it is assumed that only those two modes are active as functions of the perturbation factor δp.

$$u_1 = \alpha(\delta p), \quad u_2 = u_3 = 0, \quad u_4 = \beta(\delta p), \quad u_5 = u_6 = 0 \tag{25}$$

Hence, the governing equilibrium equations are again truncated after the quartic term and reduced to the following two equations:

$$
\begin{aligned}
\frac{\partial A}{\partial u_1} =& A_{11}^{\mathrm{F}} u_1 + \frac{1}{2}\left[A_{111}^{\mathrm{F}} u_1^2 + A_{144}^{\mathrm{F}} u_4^2\right] + \frac{1}{6} A_{1111}^{\mathrm{F}} u_1^3 + \frac{1}{2} A_{1144}^{\mathrm{F}} u_1 u_4^2 \\
& + \delta p\, A_{11}^{\prime \mathrm{F}} u_1 = 0, \\
\frac{\partial A}{\partial u_4} =& A_{44}^{\mathrm{F}} u_4 + A_{144}^{\mathrm{F}} u_1 u_4 + \frac{1}{2} A_{1144}^{\mathrm{F}} u_1^2 u_4 + \frac{1}{6} A_{4444}^{\mathrm{F}} u_4^3 + \delta p\, A_{44}^{\prime \mathrm{F}} u_4 = 0.
\end{aligned}
\tag{26}
$$

By eliminating δp in both equations the solution is projected onto the $u_1 u_4$-plane. For $p_0 = p_1^{\mathrm{C}}$ the coupled solution becomes

$$
\begin{aligned}
u_1 \underbrace{\left(\frac{A_{111}^{\mathrm{F}}}{2} - \frac{A_{144}^{\mathrm{F}} A_{11}^{\prime \mathrm{F}}}{A_{44}^{\prime \mathrm{F}}}\right)}_{a_4} + \frac{u_4^2}{u_1} \underbrace{\frac{A_{144}^{\mathrm{F}}}{2}}_{a_5} + u_1^2 \underbrace{\left(\frac{A_{1111}^{\mathrm{F}}}{6} - \frac{1}{2}\frac{A_{1144}^{\mathrm{F}} A_{11}^{\prime \mathrm{F}}}{A_{44}^{\prime \mathrm{F}}}\right)}_{a_1} & \\
+ u_4^2 \underbrace{\left(\frac{A_{1144}^{\mathrm{F}}}{2} - \frac{1}{6}\frac{A_{4444}^{\mathrm{F}} A_{11}^{\prime \mathrm{F}}}{A_{44}^{\prime \mathrm{F}}}\right)}_{a_2} = \underbrace{-\Delta p A_{11}^{\prime \mathrm{F}}}_{a_3},
\end{aligned}
\tag{27}
$$

with $\Delta p = p_4^{\mathrm{C}} - p_1^{\mathrm{C}}$. This equation has a similar form to the coupled-buckling equation for the square lattice model in Eq. (15) apart from the additional terms $a_4 u_1$ and $a_5 u_4^2/u_1$. The respective coefficients a_4, a_5 are linearly dependent on the lateral spring stiffness K.

Hence, for the case of no influence of the spring rosette, *i.e.* $K = 0$, the coupled buckling behaviour is reduced to either elliptic or hyperbolic behaviour dependent on a_1, a_2 and a_3 as already discussed in §2.5. In the vicinity of $R = 1$ ($\Delta p = 0$) it is valid that since

$$
\begin{aligned}
A_{1144}^{\mathrm{F}} &< \frac{1}{3}\frac{A_{1111}^{\mathrm{F}} A_{44}^{\prime \mathrm{F}}}{A_{11}^{\prime \mathrm{F}}} \Rightarrow a_1 > 0 \\
A_{1144}^{\mathrm{F}} &< \frac{1}{3}\frac{A_{4444}^{\mathrm{F}} A_{11}^{\prime \mathrm{F}}}{A_{44}^{\prime \mathrm{F}}} \Rightarrow a_2 < 0,
\end{aligned}
\tag{28}
$$

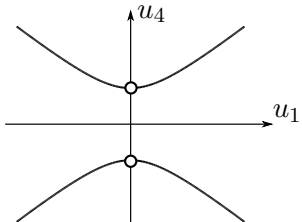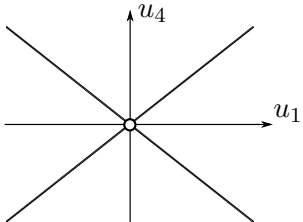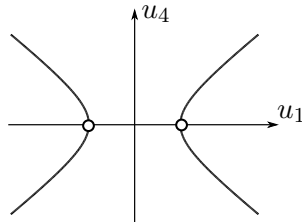the sign of Δp determines the form of interactive buckling. This is shown in the first line of Table 2.
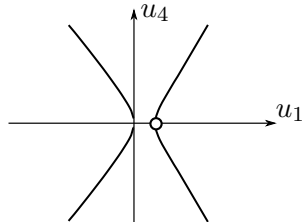
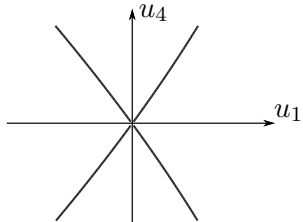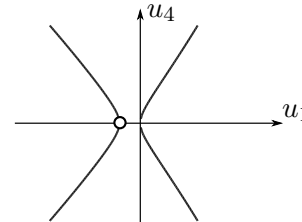|	$R < 1 (\Delta p < 0)$ mode 4 critical	$R = 1 (\Delta p = 0)$ compound branching point	$R > 1 (\Delta p > 0)$ mode 1 critical
$K = 0$	hyperbola branching from u_4-axis	straight lines going through origin	hyperbola branching from u_1-axis
$K > 0$	asymmetric branching from u_1 and u_4-axis	symmetric branching from u_4-axis	asymmetric branching from u_1 and u_4-axis

Table 2: Forms of the coupled solution for modes 1 and 4.

In the case where the energy contribution of the lateral spring rosette is taken into account, *i.e.* $K > 0$, the post-buckling response becomes asymmetric as shown in the second row of Table 2. This is owing to the influence of the linear term as well as the cubic cross term, assigned with the coefficients a_4 and a_5, which break the inherent symmetry in terms of the u_4-axis. The signs of a_4 and a_5 are given by the following conditions, since

$$
A_{111}^{\mathrm{F}} < 2A_{144}^{\mathrm{F}} \frac{A_{11}'^{\mathrm{F}}}{A_{44}'^{\mathrm{F}}} \Rightarrow a_4 < 0
$$
$$
A_{114}^{\mathrm{F}} > 0 \qquad \Rightarrow a_5 > 0.
$$

(29)

For $R \neq 1$, a secondary bifurcation point is observed along the u_1-axis while another secondary bifurcation is supposed to lie in the origin ($u_1 = u_4 = 0$). However, the truncated post-buckling solution exhibits a singularity in $u_1 = 0$ so that the analytical solution is not defined in that point. It is important to note that the coupled buckling paths remain symmetric with respect to the u_1-axis, but symmetry is lost in terms of the u_4-axis due to the influence of K. Only for the case where $R = 1$ is symmetry maintained with respect to both axes.

3.4.2. Antisymmetric modes

With higher values of K, the antisymmetric modes 2 and 5 interact. Since the central node does not deflect in this case, the non-dimensional lateral stiffness K does not in fact

contribute to the critical load expressions p_2^C and p_5^C. Assuming that only these two modes are active, which implies that the following expressions hold:

$$u_1 = 0, \quad u_2 = \alpha(\delta p), \quad u_3 = u_4 = 0, \quad u_5 = \beta(\delta p), \quad u_6 = 0, \tag{30}$$

the system is reduced to the following two equilibrium equations:

$$\begin{aligned}
\frac{\partial A}{\partial u_2} &= A_{22}^F u_2 + \frac{1}{6} A_{2222}^F u_2^3 + \frac{1}{2} A_{2255}^F u_2 u_5^2 + \delta p A_{22}'^F u_2 = 0, \\
\frac{\partial A}{\partial u_5} &= A_{55}^F u_5 + \frac{1}{2} A_{2255}^F u_2^2 u_5 + \frac{1}{6} A_{5555}^F u_5^3 + \delta p\, A_{55}'^F u_5 = 0.
\end{aligned} \tag{31}$$

Projected onto the $u_2 u_5$-plane for $p_0 = p_5^C$, the equilibrium branches of coupled buckling are described by the equation:

$$u_2^2 \underbrace{\left(\frac{1}{2} A_{2255}^F - \frac{1}{6} \frac{A_{2222}^F A_{55}'^F}{A_{22}'^F} \right)}_{a_1} + u_5^2 \underbrace{\left(\frac{1}{6} A_{5555}^F - \frac{1}{2} \frac{A_{2255}^F A_{55}'^F}{A_{22}'^F} \right)}_{a_2} = \underbrace{-\Delta p A_{55}'^F}_{a_3}, \tag{32}$$

with $\Delta p = p_2^C - p_5^C$ which resembles the post-buckling path from the square lattice model in §2.5. Herein, the coefficients a_1, a_2 evaluated close to $R = 1$ are given by:

$$\begin{aligned}
A_{2255}^F &< \frac{1}{3} \frac{A_{2222}^F A_{55}'^F}{A_{22}'^F} \Rightarrow a_1 < 0 \\
A_{2255}^F &< \frac{1}{3} \frac{A_{5555}^F A_{22}'^F}{A_{55}'^F} \Rightarrow a_2 > 0.
\end{aligned} \tag{33}$$

Hence, there remains the dependence on a_3 – more precisely on Δp – which is shown qualitatively in Table 3. Note that quantitative statements regarding the bifurcation points could be made by evaluating the coefficients for a given parameter configuration.

3.5. Comparison with AUTO-07P

The results presented hitherto are compared against results obtained with AUTO-07P [19], a well-known numerical continuation package that is able to locate bifurcation points as well as compute and switch between the associated stable and unstable branches. In accordance with Tables 2 and 3, two particular cases for $R < 1, K > 0$ and $R > 1, K > 0$ are studied in the following.

3.5.1. Case: $R = 0.98, K = 0.5$

Figure 12 clearly indicates mode interaction between modes 1 and 4, as well as between modes 2 and 5. In order to compare the analytically predicted and the numerically computed results, both curves are superimposed. This was performed for both coupled buckling phenomena and is shown in Fig. 13. Note that AUTO solves the full set of untruncated equilibrium equations numerically, whereas the analytical method solves the a reduced set of truncated equilibrium equations. This justifies the underlying assumptions presented in §3.4, thus:
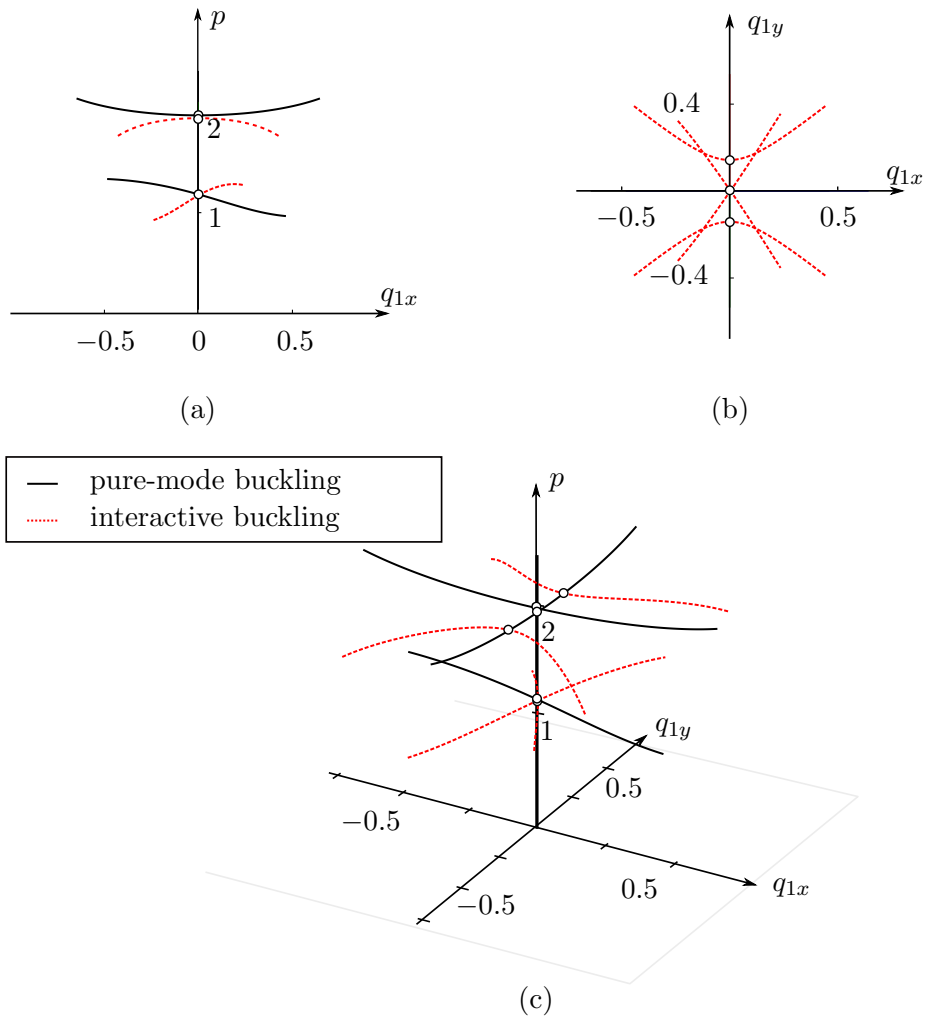
(a)

(b)

pure-mode buckling
interactive buckling

(c)

Figure 12: Coupled equilibrium paths, where $K = 0.5, R = 0.98$, generated by AUTO, showing a series of primary and secondary bifurcations.
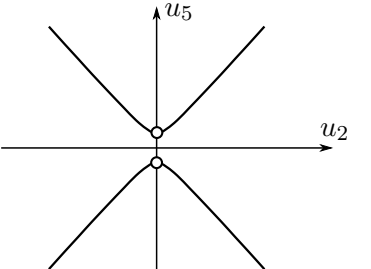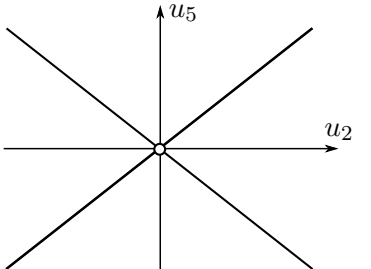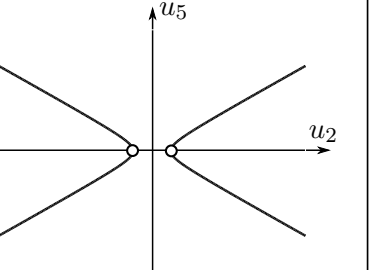
$R < 1\,(\Delta p > 0)$ mode 5 critical	$R = 1\,(\Delta p = 0)$ compound branching point	$R > 1\,(\Delta p < 0)$ mode 2 critical
hyperbola branching from u_5-axis	straight lines going through origin	hyperbola branching from u_2-axis

Table 3: Forms of the coupled solution for modes 2 and 5.

Figure 13: Comparison between the results determined numerically within AUTO and the analytical results for the case $K = 0.5, R = 0.98$: coupled forms of buckling between (a) modes 1 and 4 and (b) modes 2 and 5; the differences are not distinguishable.

- when the deformations of the structure are moderately large so that they are described sufficiently well by total potential energy terms up to and including quartic,

- in case the competing modes are separated sufficiently from the remaining modes, *e.g.* modes 1 and 4 from 2 and 5, the interactive behaviour is precisely described by a reduced set of equilibrium equations.

3.5.2. Case: $R = 1.02, K = 0.5$

For the sake of completeness the case $R > 0$ while $K > 0$ is investigated in the following Figures 14 and 15. The results found in the previous subsection are also applicable for the

Figure 14: Coupled equilibrium paths, where $K = 0.5, R = 1.02$, generated by AUTO, showing a series of primary and secondary bifurcations.

current case. Again, it is found that the comparison between the truncated energy model results and the numerical results from AUTO are barely distinguishable.
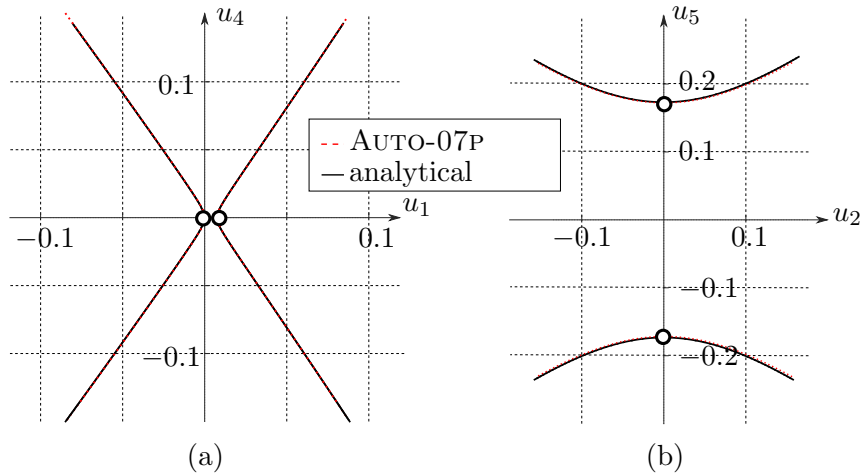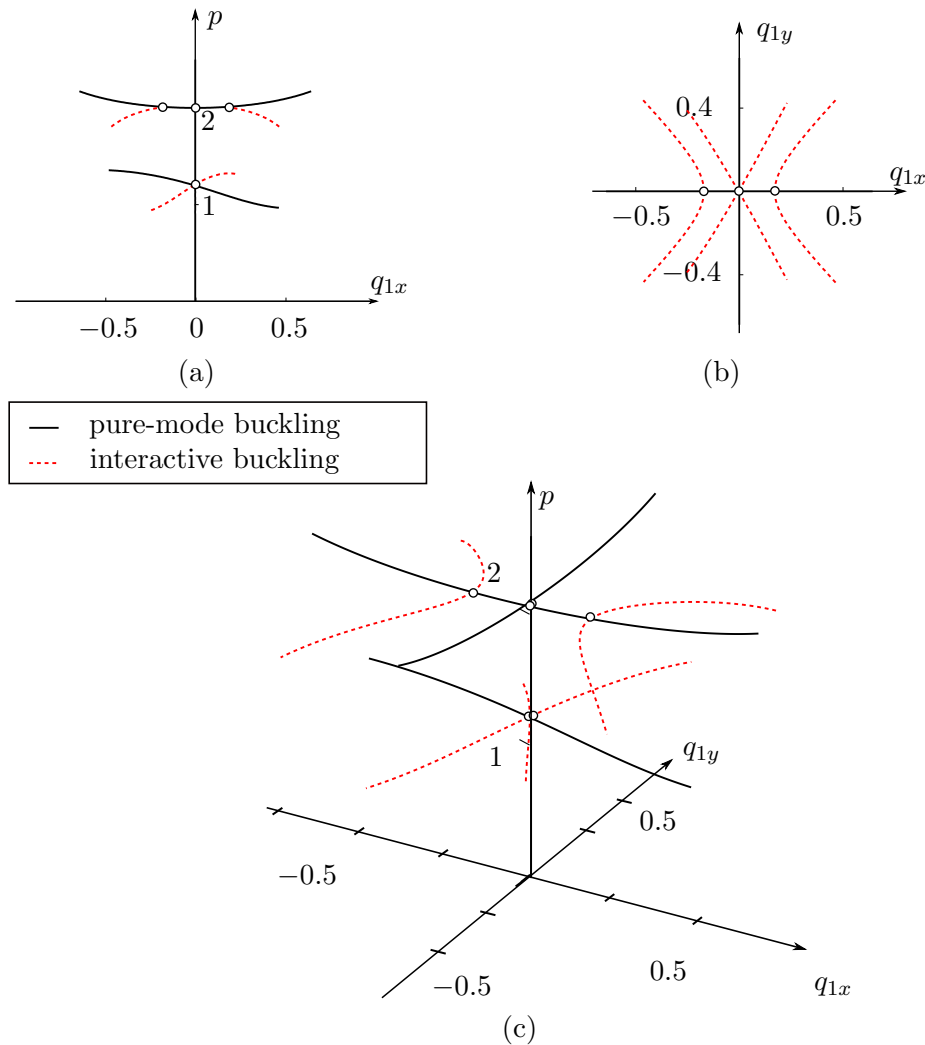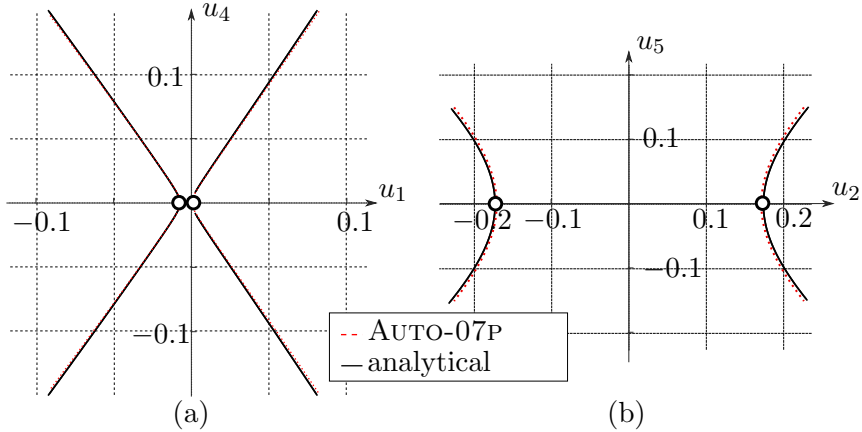
20

Figure 15: Comparison between the results determined numerically within AUTO and the analytical results for the case $K = 0.5, R = 1.02$: coupled forms of buckling between (a) modes 1 and 4 and (b) modes 2 and 5; the differences are again barely distinguishable.

3.6. More complex interactions

Following the thorough description of the coupled buckling behaviour due to the interaction of two modes, more complex mode interactions are considered. This includes the interaction of three and four modes. The inherent instabilities caused by such interactions should be particularly taken into account by the designer when reinforcing the unit cell using fibres. The following results are derived numerically with AUTO-07P.

3.6.1. Interactions between 3 modes

Interactions between three buckling modes occur so long as the buckling loads of three different modes are in close proximity. All six critical loads are plotted for $K > 0, R = 2$ in Fig. 10. The buckling loads presented in Equation (24) reveal that a three-fold modal interaction can only arise from the symmetric and antisymmetric modes in the xz-plane coupled together with the higher symmetric mode in the yz-plane or vice versa. Hence, a three-fold coupling between

- modes 1, 2 and 6 occurs for $R \to 0, K = 4/3$ or

- modes 3, 4 and 5 occurs for $R \to \infty, K = 4R/3$

is theoretically feasible. However, the rotational stiffness ratio R must therefore come close to zero or infinity. This would refer to constitutive struts with a rotationally highly asymmetric cross-section. The numerical results shown in Fig. 16 show that the post-buckling behaviour is no longer hyperbolic as it is shown in §3.4 for interactions between two modes.

3.6.2. Interactions between 4 modes

Interactive buckling behaviour due to the coincidence of four buckling modes is perfectly feasible for rotationally symmetric geometries where $R = 1$. This case leads to mode 1
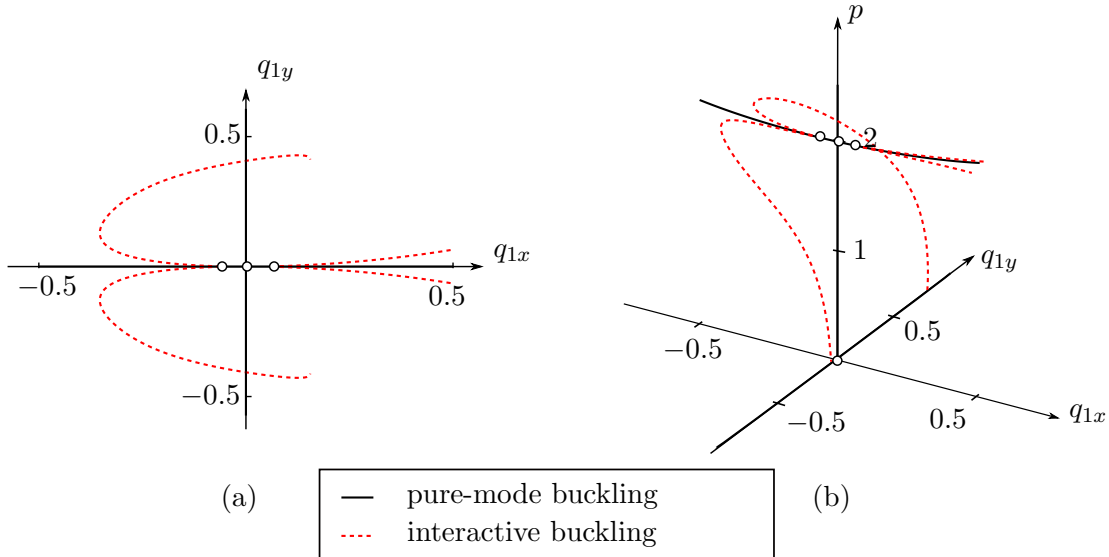
Figure 16: Coupled equilibrium paths, where $K = 4/3, R = 0.01$, generated by AUTO, showing a 3-mode interaction between mode 1, mode 2 and mode 6.

being coincident with mode 4, mode 2 with mode 5 and mode 3 with mode 6. As shown in Fig. 10, as soon as the normalized lateral spring stiffness reaches $K = 4/3$, the critical loads of modes 1, 2, 4 and 5 are coincident. The numerical results from AUTO by solving the full set of equilibrium equations numerically leads to the results presented in Fig. 17.

However, these situations where interactions between three and four buckling modes can be prevented by avoiding the specific conditions for the stiffness parameters K and R respectively by pre-designing the lattice structural geometry.

4. Discussion and Outlook

The work presented is part of a multi-scale design process of truss-based lattice materials. The aim has been to address the problem of finding effective material parameters at the cell level by modelling the deformational behaviour of a single unit cell analytically. This is necessary as the well-known scaling laws given in [5] are only applicable for stochastic cellular materials, so that new methods for periodically structured lattice materials need to be developed. Furthermore, the analytical approach promotes the fundamental understanding of the elastic failure mechanisms within the individual unit cells. As a means to influence the behaviour of such unit cells additionally, the use of fibres has been proposed.

Discrete models of two different fibre-reinforced unit cells – a two-dimensional cross-shaped cell and a three-dimensional tetrahedron-shaped cell – have subsequently been developed. Against the background of the aforementioned experimentally observed stability problems for lattice materials under compression, as shown for instance in Fig. 1(b), both models have been evaluated within the elastic range. The evaluation of the total potential energy led to the determination of a series of buckling loads triggering different modes in terms of the model parameters. The influence of the interwoven fibres, modelled
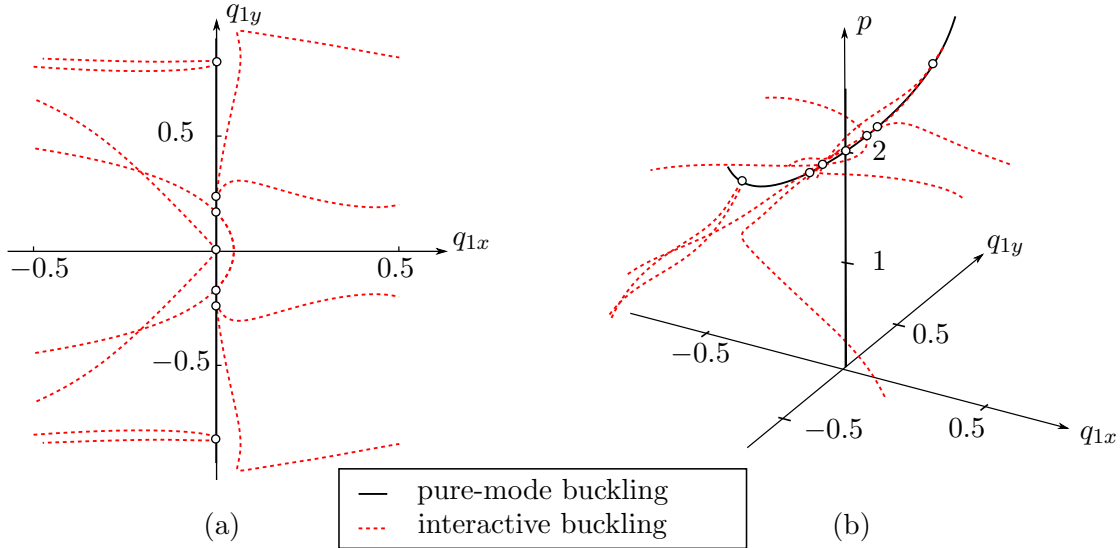
22

Figure 17: Coupled equilibrium paths, where $K = 4/3, R = 0.98$, generated by AUTO, showing a 4-mode interaction between mode 1, mode 2, mode 4 and mode 5.

with the normalized longitudinal spring stiffness K, being identified herein as a crucially important parameter.

Even though both models provide valuable results for the respective geometries, it could be argued that a comparison between them has only limited value. Apart from the difference in dimensions, the cross-shaped model respects fully fixed boundary conditions due to the face-sheets whereas the tetrahedron-shaped model imposes no rotational constraint on the outer links. Furthermore, the two-dimensional model considers buckling of the cross-member. This leads to an interaction between symmetric and antisymmetric buckling modes at a considerably higher K value when compared to the tetrahedron-shaped model. The results for the latter model showed good qualitative agreement nevertheless with previous work from [13]; where analysis was conducted on a symmetric two-dimensional link model that behaved in a similar fashion to those presented currently (apart from the fact that the three-dimensional tetrahedron-shaped unit cell model buckles in two dimensions).

Furthermore, both models provided significant results for their post-buckling behaviour. Parametric studies performed on the governing model parameters revealed several forms of post-buckling including nonlinear modal interactions. These were analysed using a perturbation method on the truncated potential energy and results were subsequently compared against solutions of the full model from AUTO-07P. These showed excellent agreement for the interaction between two modes even for relatively large displacements. Interactions between more than two modes have been found to exhibit more complex behaviour. It has been demonstrated that the interactions between three modes can only practically occur in exceptional geometries. However, interactions between four buckling modes are quite feasible, in particular for rotationally symmetric unit cells.

While the application of the current methodology has been demonstrated for modelling the constitutive elements of lattice materials within the elastic range, additional work needs

to be conducted in order to increase their practicality. Elastic instability provides only an upper bound for slender geometries. In the first instance, the consideration of plastic buckling failure within the model would enable the definition of a lower bound for less slender geometries. Considerable groundwork may be found in earlier analytical studies by Hunt [20], where the Shanley model for plastic buckling of columns [21] was adapted and an equivalent elastic model was formulated. Serially arranged springs were manipulated and the post-buckling behaviour changed qualitatively. Secondly, the aforementioned findings for the unit cell need to be scaled to the macroscopic scale level to find the effective material parameters and hence the constitutive relationship that can be applied in design. This can be achieved by connecting several unit cells in a grid. The constraints imposed on the boundary of the respective cell need to depend on the neighbouring elements in this case. Therefore, the current work marks a point of departure from where more complex analytical models could be evaluated with the energy principles applied presently. The finite element (FE) method is likely to be very useful for investigating larger lattices in conjunction with the analytical formulations. The analytical framework would facilitate the understanding how individual unit cells influence the global behaviour of the lattice material; the global behaviour being studied principally using FE.

Apart from the mentioned model extensions, additional work could be conducted constructing prototypes with prestressed fibres and investigating them experimentally. Considering the production, this could be achieved using a lay-up process similar to [6], where the fibres would be interwoven within the single layers and prestressed subsequently prior to bonding. Although, to the authors' knowledge this has not been attempted before, the potential is highly promising as the presented analytical considerations and previous work on prestressed compression members have demonstrated [10, 11].

5. Concluding remarks

A couple of fibre-reinforced materials have been proposed. One is based on a square orientated lattice material with a cross-shaped unit cell that has been modelled in two dimensions using rigid links and springs. The second is a tetrahedron-shaped unit cell and has been modelled discretely in three dimensions. The geometrically nonlinear behaviour under compression has been analysed through the principles of minimum total potential energy.

Both models have been demonstrated to be successful in exhibiting the experimentally observed vulnerability to instability that is dependent on the unit cell geometry. The application of a perturbation method on a truncated potential energy expression provided significant results for the behaviour in the post-buckling range. In particular, the methodology was demonstrated to be an effective analytical tool for determining and classifying modal interactions. Cases have been presented for both geometries showing different forms of interactive buckling dependent on the geometric properties. Whereas numerical techniques, *e.g.* the FE method, would require the introduction of imperfections to demonstrate the same physical responses [22].

The post-buckling response of the unit cells could be manipulated by means of the results presented. This could be practically useful for determining the large scale constitutive behaviour in the conceptual design stages. Therefore, further research into the quantitative assignment of the model parameters is necessary and suggestions using the FE method in conjunction with developing prestressed prototypes have been outlined.

Appendix A. Diagonalizing transformation

For the tetrahedron-shaped unit cell model, the original generalized coordinates q_{ix}, q_{iy} for $i = \{1, 2, 3\}$ are defined in terms of new coordinates u_j for $j = \{1, 2, \ldots, 6\}$, thus:

$$\begin{aligned}
q_{1x} &= u_1 + u_2 + u_3 \\
q_{1y} &= u_4 + u_5 + u_6 \\
q_{2x} &= \lambda_1 u_1 - \lambda_3 u_3 \\
q_{2y} &= \lambda_4 u_4 - \lambda_6 u_6 \\
q_{3x} &= u_1 - u_2 + u_3 \\
q_{3y} &= u_4 - u_5 + u_6.
\end{aligned} \tag{A.1}$$

The values of λ_i for $i = \{1, 3, 4, 6\}$ are assigned based on the condition that no quadratic cross terms $u_i u_j$ (for $i \neq j$) should appear in the total potential energy formulation; this leads to the following relationships in terms of K and R:

$$\begin{aligned}
\lambda_1 &= \frac{3K - \sqrt{9K^2 + 32 - 24K}}{3K - 4} \\
\lambda_3 &= \frac{\lambda_1 - 2}{1 - \lambda_1}, \\
\lambda_4 &= \frac{3K - \sqrt{9K^2 + 32R^2 - 24RK}}{3K - 4R}, \\
\lambda_6 &= \frac{\lambda_4 - 2}{1 - \lambda_4}.
\end{aligned} \tag{A.2}$$

Appendix B. Diagonal elements of Hessian Matrix A

The Hessian matrix of $\mathbf{A}$ for the model of the tetrahedron-shaped unit cell has the following elements:

$$
\begin{aligned}
A_{11}^{\mathrm{F}} &= \lambda_1^2 \left(6 + \frac{3}{2}K - 2p \right) + \lambda_1 \left(4p - 16 \right) + 12 - 4p \\
A_{22}^{\mathrm{F}} &= 8 - 4p \\
A_{33}^{\mathrm{F}} &= \lambda_3 \left(6 + \frac{3}{2}K - 2p \right) + \lambda_3 \left(16 - 4p \right) + 12 - 4p \\
A_{44}^{\mathrm{F}} &= \lambda_4^2 \left(6R + \frac{3}{2}K - 2p \right) + \lambda_4 \left(4p - 16R \right) + 12R - 4p \\
A_{55}^{\mathrm{F}} &= 8R - 4p \\
A_{66}^{\mathrm{F}} &= \lambda_6^2 \left(6R + \frac{3}{2}K - 2p \right) + \lambda_6 \left(16R - 4p \right) + 12R - 4p.
\end{aligned}
\tag{B.1}
$$

Appendix C. Eigenvectors of buckling modes

The critical buckling eigenvectors associated with the eigenvalues p_i^{C} for the tetrahedron-shaped unit cell model are denoted as $\vec{a}_i$ for $i = \{1, 2, \ldots, 6\}$ thus:

$$
\begin{aligned}
\vec{a}_1 &= [1, 0, \lambda_1, 0, 1, 0]^T \\
\vec{a}_2 &= [-1, 0, 0, 0, 1, 0]^T \\
\vec{a}_3 &= \left[\frac{3K-4}{8}\lambda_1, 0, 1, 0, \frac{3K-4}{8}\lambda_1, 0 \right]^T \\
\vec{a}_4 &= [0, 1, 0, \lambda_4, 0, 1]^T \\
\vec{a}_5 &= [0, -1, 0, 0, 0, 1]^T \\
\vec{a}_6 &= \left[0, \frac{3K-4R}{8R}\lambda_4, 0, 1, 0, \frac{3K-4R}{8R}\lambda_4 \right]^T.
\end{aligned}
\tag{C.1}
$$

References

[1] M. F. Ashby, A. G. Evans, N. A. Fleck, L. J. Gibson, J. W. Hutchinson, H. N. G. Wadley, Metal Foams, Butterworth-Heinemann, Burlington, 2000.

[2] N. A. Fleck, V. S. Deshpande, M. F. Ashby, Micro-architectured materials: past, present and future, Proceedings of the Royal Society A 466 (2121) (2010) 2495–2516.

[3] J. Tian, T. Lu, H. Hodson, D. Queheillalt, H. Wadley, Cross flow heat exchange of textile cellular metal core sandwich panels, International Journal of Heat and Mass Transfer 50 (13–14) (2007) 2521–2536.

[4] O. Rehme, Cellular Design for Laser Freeform Fabrication, Schriftenreihe Lasertechnik, Cuvillier, 2010.

[5] L. J. Gibson, M. F. Ashby, Cellular Solids: Structure and Properties, Cambridge Solid State Science Series, Cambridge University Press, 1999.

[6] D. T. Queheillalt, H. N. Wadley, Cellular metal lattices with hollow trusses, Acta Materialia 53 (2) (2005) 303–313.

[7] L. Gao, Y. Sun, L. Cong, P. Chen, Mechanical behaviours of composite sandwich panel with strengthened pyramidal truss cores, Composite Structures 105 (0) (2013) 149–152.

[8] E. Belenya, Prestressed load-bearing metal structures, Mir Publishers, 1977.

[9] H. H. Hafez, M. C. Temple, J. S. Ellis, Pretensioning of single-crossarm stayed columns, ASCE Journal of the Structural Division 105 (ST 2) (1979) 359–375.

[10] D. Saito, M. A. Wadee, Post-buckling behaviour of prestressed steel stayed columns, Engineering Structures 30 (5) (2008) 1224–1239.

[11] D. Saito, M. A. Wadee, Numerical studies of interactive buckling in prestressed steel stayed columns, Engineering Structures 31 (2) (2009) 432–443.

[12] A. I. Osofero, M. A. Wadee, L. Gardner, Experimental study of critical and post-buckling behaviour of prestressed stayed columns, Journal of Construnctional Steel Research 79 (2012) 226–241.

[13] M. A. Wadee, L. Gardner, T. A. Hunt, Buckling mode interaction in prestressed stayed columns, Proceedings of the Institution of Civil Engineers: Structures and Buildings 166 (2013) 403–412.

[14] G. W. Hunt, Bifurcations of structural components, Proceedings of the Institution of Civil Engineers Part 2 87 (1989) 443–467.

[15] J. M. T. Thompson, G. W. Hunt, A general theory of elastic stability, Wiley, London, 1973.

[16] W. J. Supple, Coupled branching configurations in the elastic buckling of symmetric structural systems, International Journal of Mechanical Sciences 9 (2) (1967) 97–112.

[17] A. H. Chilver, Coupled modes of elastic buckling, Journal of the Mechanics and Physics of Solids 15 (1) (1967) 15–28.

[18] C. O'Sullivan, M. A. Wadee, K. J. Hanley, D. Barreto, Use of DEM and elastic stability analysis to explain the influence of the intermediate principal stress on shear strength, Geotechnique 63 (2013) 1298–1309.

[19] E. J. Doedel, B. E. Oldeman, Auto-07p: Continuation and bifurcation software for ordinary differential equations, Tech. rep., Department of Computer Science, Concordia University, Montreal, Canada, available from `http://indy.cs.concordia.ca/auto/` (2009).

[20] G. W. Hunt, B. A. Burgan, Hidden asymmetries in the shanley model, Journal of the Mechanics and Physics of Solids 33 (1) (1985) 83–94.

[21] F. R. Shanley, Inelastic column theory, Journal of the Aeronautical Sciences 14 (5) (1947) 261–268.

[22] T. Belytschko, W. K. Liu, B. Moran, Nonlinear finite elements for continua and structures, Wiley, Chichester, 2000.